# Gas-particle partitioning of polyol tracers at a suburban site in Nanjing, east China: Increased partitioning to the particle phase

Chao Qin[a], Yafeng Gou[b], Yuhang Wang[c], Yuhao Mao[b], Hong Liao[b], Qin'geng Wang[d], Mingjie Xie[b,*]

[a] Colleges of Resources and Environmental Sciences, Nanjing Agricultural University, Nanjing 210095, China

[b] Collaborative Innovation Center of Atmospheric Environment and Equipment Technology, Jiangsu Key Laboratory of Atmospheric Environment Monitoring and Pollution Control, School of Environmental Science and Engineering, Nanjing University of Information Science & Technology, 219 Ningliu Road, Nanjing 210044, China

[c] School of Earth and Atmospheric Sciences, Georgia Institute of Technology, Atlanta, GA 30332

[d] State Key Laboratory of Pollution Control and Resources Reuse, School of the Environment, Nanjing University, Nanjing 210023, China

*Corresponding to:

Mingjie Xie (mingjie.xie@nuist.edu.cn; mingjie.xie@colorado.edu);

Tel: +86-18851903788l; Fax: +86-25-58731051;

Mailing address: 219 Ningliu Road, Nanjing, Jiangsu, 210044, China

**Abstract**

Gas-particle partitioning of water-soluble organic compounds plays a significant role in influencing the formation, transport, and lifetime of organic aerosols in the atmosphere, but is poorly characterized. In this work, gas- and particle-phase concentrations of isoprene oxidation products (C5-alkene triols and 2-methylterols), levoglucosan, and sugar polyols were measured simultaneously at a suburban site of the western Yangtze River Delta in east China. All target polyols were primarily distributed into the particle phase (85.9–99.8%). Given the uncertainties in measurements and vapor pressure predictions, a dependence of particle-phase fractions on vapor pressures cannot be determined. To explore the impact of aerosol liquid water on gas-particle partitioning of polyol tracers, three partitioning schemes (*Cases 1-3*) were proposed based on equilibriums of gas versus organic and aqueous phases in aerosols. If particulate organic matter (OM) is presumed as the only absorbing phase (*Case 1*), the measurement-based absorptive partitioning coefficients ($K^{m}_{p,OM}$) of isoprene oxidation products and levoglucosan were more than 10 times greater than predicted values ($K^{t}_{p,OM}$). The agreement between $K^{m}_{p,OM}$ and $K^{t}_{p,OM}$ was substantially improved when solubility in a separate aqueous phase was included, whenever water-soluble and water-insoluble OM partitioned into separate (*Case 2*) or single (*Case 3*) liquid phases, suggesting that the partitioning of polyol tracers into the aqueous phase in aerosols should not be ignored. The measurement-based effective Henry's law coefficients ($K^{m}_{H,e}$) of polyol tracers were orders of magnitude higher than their predicted values in pure water ($K^{t}_{H,w}$). Due to the moderate correlations between log ($K^{m}_{H,e}/K^{t}_{H,w}$) and molality of sulfate ions, the gap between $K^{m}_{H,e}$ and $K^{t}_{H,w}$ of polyol tracers could not be fully parameterized by the equation defining

54 “salting-in” effects, and might be ascribed to mechanisms of reactive uptake, aqueous
55 phase reaction, “like-dissolves-like” principle, etc. These study results also partly
56 reveals the discrepancy between observation and modeling of organic aerosols.
57
58
59
60
61
62
63
64
65
66
67
68
69
70
71
72
73
74
75
76

## 1 Introduction

The water-soluble organic carbon (WSOC) in ambient aerosols can account for 20-80% of particulate organic matter (OM) based on carbon mass (Saxena and Hildemann, 1996; Kondo et al., 2007). Field studies on the hygroscopic growth and cloud condensation nucleus (CCN) activity of aerosol extracts indicated that WSOC contributed significantly to aerosol hygroscopicity, and modified the hydration behavior of inorganic species (e.g., sulfate, nitrate, and ammonium; Hallar et al., 2013; Taylor et al., 2017). Thus, WSOC plays an important role in changing radiative and cloud nucleating properties of atmospheric particles. Particulate WSOC is a complex mixture of polar organic compounds containing oxygenated functional groups (e.g., hydroxyl, carboxyl, and carbonyl groups), among which a list of organic compounds with multiple hydroxyl (polyols) groups have been identified using gas chromatography -mass spectrometry (GC-MS) and linked with specific emission sources. For example, C5-alkene triols and 2-methyltetrols are isoprene oxidation products (Claeys et al., 2004; Wang et al., 2005; Surratt et al., 2006); levoglucosan is a typical pyrolysis product of cellulose (Simoneit et al., 1999); primary saccharides (e.g., fructose and glucose) and saccharide polyols (e.g., arabitol and mannitol) are commonly associated with soil microbiota and fungal spores, respectively (Simoneit et al., 2004; Bauer et al., 2008).

To quantify the sources contributing to WSOC, concentrations of individual organic tracers are often used as inputs for receptor-based modeling (Zhang et al., 2009; Hu et al., 2010). Due to the influences of gas-particle partitioning on source apportionment, Xie et al. (2013, 2014c) suggested the involvement of gas-phase concentrations of organic makers through theoretical prediction or field measurements.

The equilibrium absorptive partitioning theory outlined by Pankow (1994a, b) and laboratory measurements of secondary organic aerosol (SOA) yields (Odum et al., 1996) have been widely applied to predict SOA formation in traditional modeling studies (Heald et al., 2005; Volkamer et al., 2006; Hodzic et al., 2010). In addition to absorptive partitioning to particulate OM after the formation of oxygenated organic compounds in gas phase, other formation pathways (e.g., reactive uptake) have been identified and are responsible for the large discrepancy between modeled and observed SOA loadings (Jang et al., 2002; Kroll et al., 2005; Perraud et al., 2012). Unlike non-polar species (e.g., *n*-alkanes, polycyclic aromatic hydrocarbons) and alkanoic acids that are well simulated (Simcik et al., 1998; Xie et al., 2014a; Yatavelli et al., 2014; Isaacman-VanWertz et al., 2016), particle-phase concentrations of carbonyls were underestimated by several orders of magnitude when particulate OM is presumed as the only absorbing phase in ideal condition (Healy et al., 2008; Kampf et al., 2013; Shen et al., 2018). Zhao et al. (2013) observed a positive dependence of particle-phase pinonaldehyde on relative humidity (RH, %), and inferred that aerosol water played a role in the formation of pinonaldehyde in the atmosphere. However, very few studies have been performed on the measurement of gaseous polyols (Xie et al., 2014b; Isaacman-VanWertz et al., 2016), and their gas-particle partitioning were poorly understood.

Henry's law can describe the uptake of a compound into a liquid, highly dilute solution (e.g., cloud droplets) in the atmosphere (Ip et al., 2009; Compernolle and Müller, 2014a). Aerosol water is also a major component of atmospheric particles, and accounts for 40% by volume at 50% RH in Europe (Tsyro, 2005). But the bulk aerosol solution is highly concentrated with inorganic ions and WSOC. An effective

Henry's law coefficient ($K_{H,e}$, mol $m^{-3}$ $atm^{-1}$) can be used to account for the measured partitioning between the gas phase and aerosol liquid water (Volkamer et al., 2009). Both laboratory and field studies observed enhanced $K_{H,e}$ of carbonyl compounds with inorganic salt concentrations (in mol $kg^{-1}$ aerosol liquid water content, ALWC; Kampf et al., 2013; Waxman et al., 2015; Shen et al., 2018). This "salting-in" effect (Setschenow, 1889) is not mechanistically understood, and might be linked with the hydrophilic interactions (e.g., hydrogen bonding) between polar organic compounds and inorganic ions leading to an increase of entropy or decrease of Gibbs free energy (Almeida et al., 1983; Waxman et al., 2015). Polyol tracers are highly water-soluble and their gas-particle partitioning is very likely driven by the aqueous phase containing substantial ionic species in ambient aerosols. In the Southeastern US, the particle-phase fraction (*F*%) of WSOC is highly dependent on RH and ALWC (Hennigan et al., 2009).

In the present study, polyols related to specific emission sources in gaseous and particle phases were measured concurrently in northern Nanjing, China. The sampling and chemical analysis were performed in a similar manner as Xie et al. (2014b), while an additional step was added prior to GC-MS analysis to clean the extracts of gaseous samples. To explore the roles of aerosol liquid water on gas-particle partitioning of polyol tracers, three modes (*Cases 1-3*) were proposed based on equilibriums between gas and liquid aerosol phases, and the measurement-based and predicted partitioning coefficients were compared across individual cases. This work tends to explain the gas-particle partitioning of polyols at a suburban site in eastern China, where the estimated average mass concentration of aerosol liquid water is close to 20 μg $m^{-3}$ (Yang et al., 2021).

## 2 Methods

### *2.1 Field Sampling*

Details of the sampling information were provided in Yang et al. (2021). Briefly, ambient air was sampled on the rooftop of a seven-story library building located in Nanjing University of Information Science and Technology (NUIST 32.21 $^{o}$N, 118.71 $^{o}$E), a suburban site in the western Yangtze River Delta of east China. A medium volume sampler (PM-PUF-300, Mingye Environmental, Gugangzhou, China) equipped with a 2.5 μm cut impactor was configured to collect particulate matter with aerodynamic diameter less than 2.5 μm ($PM_{2.5}$) and gaseous organic compounds at a flow rate of 300 L $min^{-1}$. After the impactor, the sampled air flowed through a filter pack containing two stacked pre-baked (550 $^{o}$C, 4 h) quartz filters (20.3 cm × 12.6 cm, Munktell Filter AB, Sweden) and a polyurethane foam (PUF, 65 mm diameter × 37.5 mm length) cartridge in series. The top quartz filter ($Q_f$) in the filter pack was loaded with $PM_{2.5}$; gaseous organic compounds adsorbed on the backup quartz filter ($Q_b$) were determined to evaluate sampling artifacts; and the PUF cartridge was used for the sampling of gaseous polyols. Filter and PUF samples were collected every sixth day during daytime (8:00 AM – 7:00 PM) and night time (7:00 PM – 7:00 AM next day), respectively, from 09/28/2018 to 09/28/2019. Collection efficiency of gaseous polyols were examined by performing breakthrough experiments using two PUF plugs during nine sampling intervals. Prior to sampling, PUF adsorbents were cleaned and dried in the same way as Xie et al. (2014b). Field blank filter and PUF materials were collected every $10^{th}$ sample for contamination adjustment. Filter and PUF samples were sealed in prebaked aluminum foil and glass jars, respectively, at – 20 $^{o}$C until analysis.

### *2.2 Chemical Analysis*

**Bulk speciation.** The accumulated $PM_{2.5}$ mass and bulk components including water soluble ions ($NH_4^+$, $SO_4^{2-}$, $NO_3^-$, $Ca^{2+}$, $Mg^{2+}$, and $K^+$), organic (OC) and elemental carbon (EC), and WSOC were measured for each filter sample. Their final concentrations were determined by subtracting measurement results of $Q_b$ from those of $Q_f$. Concentrations of aerosol liquid water were predicted by ISORROPIA II model using ambient temperature, RH, and concentration data of $NH_4^+$, $SO_4^{2-}$, and $NO_3^-$ under the metastable state. The estimated water content contributed by hygroscopic WSOC was relatively small (< 1 μg $m^{-3}$) and not accounted for in this work (Text S1 of supplementary information). Table S1 lists averages and ranges of ambient temperature, RH, measured $PM_{2.5}$ components, and predicted aerosol liquid water from Yang et al. (2021).

**Polyols analysis.** Details of the analysis method for gaseous and particulate polyols were provided in supplementary information (Text S2). Briefly, 1/8 of each filter sample was pre-spiked with deuterated internal standard and extracted ultrasonically twice for 15 min in 10–15 mL of methanol and methylene chloride mixture (1:1, v/v). After filtration, rotary evaporation, $N_2$ blown down to dryness, and reaction with 50 μL of N, O-bis(trimethylsilyl)trifluoroacetamide (BSTFA) containing 1% trimethylchlorosilane (TMCS) and 10 μL of pyridine, the derivatives of polyols were diluted to 400 μL using pure hexane for GC-MS analysis. Pre-spiked PUF samples were Soxhlet extracted using a mixture of 225 mL of methylene chloride and 25 mL of methanol, followed by the same procedures of filter sample pretreatment. Prior to GC-MS analysis, 50 μL of pure water was added to precipitate PUF impurities from the final extract. As shown in Figure S1e, all PUF residues are kept in aqueous phase

at the bottom of the vial, while the derivatives of polyol tracers are supposed to be retained in the top clear hexane solution. An aliquot of 2 μL of the supernatant was injected for GC-MS analysis under splitless mode, and an internal standard method with a six-point calibration curve (0.05–5 ng $\mu L^{-1}$) was performed to quantify polyols concentrations. In this work, isoprene SOA products, including three C5-alkene triols (cis-2-methyl-1,3,4-trihydroxy-1-butene, 3-methyl-2,3,4-trihydroxy-1-butene, and trans-2-methyl-1,3,4-trihydroxy-1-butene; abbreviated as C5-alkene 1, 2, and 3) and two 2-methyltetrols (2-methylthreitol and 2-methylerythritol), were quantified using meso-erythritol; other polyols were determined using authentic standards.

Analytical recoveries of target polyols were obtained by adding known amounts of standards to blank sampling materials (quartz filter and PUF), followed by extraction and instrumental analysis identically as ambient samples. Method detection limits (MDL) of individual species were estimated as three times the standard deviation of their concentrations determined from six injections of the lowest calibration standard. Table S2 lists recovery and MDL values of authentic standard compounds. Concentrations of polyols in field blank samples were measured and subtracted from air samples if necessary. To obtain appropriate gas-particle distribution of polyol tracers, their field-blank corrected concentrations in filter and PUF samples were adjusted by recoveries. Final concentrations of individual polyols in $Q_f$, $Q_b$, and PUF samples are summarized in Table S3.

### *2.3 Data analysis*

**Gas-particle separation and breakthrough calculation.** Polyol tracers detected in $Q_b$ samples are contributed by both gaseous adsorption ("positive artifact") and particle-phase evaporation from $Q_f$ samples ("negative artifact"), but their relative

contributions are unknown. Xie et al. (2014b) adjusted particle- and gas-phase concentrations of levoglucosan and 2-methyltetrol based on $Q_b$ measurements in two different ways. One assumed that $Q_b$ values were completely attributed to gaseous adsorption; the other presumed equal contributions from gaseous adsorption and $Q_f$ evaporation. However, negligible difference in gas-particle distribution was observed due to the small $Q_b$ values. In Table S3, concentrations of polyol tracers on $Q_b$ are far below those on $Q_f$, and it would be safe to presume equal positive and negative artifacts. In this study, particle-phase concentrations of polyols were represented by $Q_f$ values, and the gas phase was calculated as the sum of $Q_b$ and PUF measurements.

The sampling efficiency of target polyols were evaluated by collecting and analyzing tandemly installed PUF plugs during nine sampling intervals. The breakthrough of each polyol was calculated as

$$B = \frac{[\mathrm{PUF}]_{\mathrm{back}}}{[\mathrm{PUF}]_{\mathrm{front}}+[\mathrm{PUF}]_{\mathrm{backup}}} \times 100\% \quad (1)$$

where $B$ is the breakthrough of gaseous sampling, and [PUF] represents the concentration of specific compound in front or backup PUF sample. A value of 33% was typically used to indicate excessive breakthrough (Peters et al., 2000; Ahrens et al., 2011).

**Calculations of partitioning coefficients**. Here, we defined three partitioning cases to explore the influence of dissolution in aerosol liquid water on gas-particle partitioning of polyol tracers in the atmosphere. *Case 1* presumes instantaneous equilibrium between the gas phase and particulate OM based on the equilibrium absorptive partitioning theory. In this case, particulate OM is assumed to be the only absorbing phase and behave as an ideal solution. Then the absorptive gas-particle partitioning coefficients ($K_{\mathrm{p,OM}}$, $\mathrm{m^3\,\mu g^{-1}}$) were calculated from measurements ($K^{\mathrm{m}}_{\mathrm{p,OM}}$)

and predicted theoretically ($K^{t}_{p,OM}$) as follows

$$K^{m}_{p,OM} = \frac{F/M_{OM}}{A} \quad (2)$$

$$K^{t}_{p,OM} = \frac{RT}{10^{6}\overline{MW}_{OM}\zeta_{OM}p^{o}_{L}} \quad (3)$$

where $M_{OM}$ denotes the mass concentration of absorptive organic matter (OM = OC × 1.6; Turpin and Lim, 2001); $F$ (ng m$^{-3}$) and $A$ (ng m$^{-3}$) are particulate and gaseous concentrations of individual polyols, respectively. In eq 3, R (m$^3$ atm K$^{-1}$ mol$^{-1}$) and T (K) are the ideal gas constant and ambient temperature; $\overline{MW}_{OM}$, average molecular weight of absorptive OM, is set at 200 g mol$^{-1}$ for all samples (Barsanti and Pankow, 2004; Williams et al., 2010); $\zeta_{OM}$ denotes the mole fraction scale activity coefficient, and is presumed to be unity for all species in each sample; $p^{o}_{L}$ (atm) is the vapor pressure of each pure compound, and is predicted with several estimation tools and adjusted for each sampling interval based on the average temperature (Text S3 and Table S4).

Due to the influence of mixing state and water content in aerosols, several studies modeled the gas-particle partitioning of oxygenated organic compounds by defining a liquid-liquid phase separation (LLPS) in the aerosol (Zuend and Seinfeld, 2012; Pye et al., 2018). The organic-inorganic interactions and changes of activity coefficients in aqueous mixtures were fully considered as well. In this study, we proposed a simplified LLPS partitioning mechanism (*Case 2*) in Figure 1. First, aerosol water and water-insoluble OM (WIOM = OM – WSOC × 1.6) exist in two separate liquid phases, and WSOC and inorganic ions are totally dissolved in the aqueous phase. The distribution of polyol tracers between aqueous ($F_W$, ng m$^{-3}$) and WIOM ($F_{WIOM}$, ng m$^{-3}$) phases is simply depicted by their octanol-water partition coefficients ($K_{OW}$)

$$K_{\mathrm{OW}} = \frac{F_{\mathrm{WIOM}}/V_{\mathrm{WSIOM}}}{F_{\mathrm{w}}/V_{\mathrm{w}}} = \frac{c_{\mathrm{WIOM}}}{c_{\mathrm{w}}} \quad (4)$$

where $V_{\mathrm{WIOM}}$ and $V_{\mathrm{w}}$ are volumes ($m^3$) of WIOM and water in aerosols per cubic meter air; $c_{\mathrm{WIOM}}$ and $c_{\mathrm{w}}$ are solution concentrations (ng $m^{-3}$) of polyols concentrations in organic and aqueous phases; log $K_{\mathrm{OW}}$ values of target polyols were estimated using the Estimation Programs Interface (EPI) Suite developed by the US Environmental Protection Agency and Syracuse Research Corporation (Table S4; US EPA, 2012). The density of organic matter and water ($\rho_{\mathrm{w}}$) in aerosols are set at 1.4 and 1.0 g $cm^{-3}$, respectively (Isaacman-VanWertz et al., 2016; Taylor et al., 2017). Second, gas-phase polyol tracers are in equilibrium with hydrophobic OM and the aqueous phase, respectively

$$K^{\mathrm{m}}_{\mathrm{p,WIOM}} = \frac{F_{\mathrm{WIOM}}/M_{\mathrm{WIOM}}}{A} \quad (5)$$

$$K^{\mathrm{m}}_{\mathrm{H,e}} = \frac{\frac{F_w}{M_i}}{\frac{A}{M_i}\times R\times T\times\frac{c_{\mathrm{ALW}}}{\rho_{\mathrm{w}}}} = \frac{\rho_{\mathrm{w}}\times F_w}{A\times R\times T\times c_{\mathrm{ALW}}} \quad (6)$$

where $K^{\mathrm{m}}_{\mathrm{H,e}}$ (mol $m^{-3}$ $atm^{-1}$) is the measurement-based effective Henry's law coefficient; $M_{\mathrm{WIOM}}$ represents the mass concentration (μg $m^{-3}$) of WIOM; $M_i$ (g $mol^{-1}$) is the molecular weight of specific compound; $c_{\mathrm{ALW}}$ (μg $m^{-3}$) is the mass concentration of aerosol liquid water predicted using ISORROPIA II model. *Case 3* is generally the same as *Case 2*, and the only difference is that water-soluble OM (WSOM) and WIOM exist in a single organic phase. Here total particulate OM was used instead of WIOM to assess the distribution of polyol tracers between aqueous and organic phases, and calculate partitioning coefficients of gas vs. particulate organic ($K^{\mathrm{m}}_{\mathrm{p,OM}}$) and aqueous ($K^{\mathrm{m}}_{\mathrm{H,e}}$) phases. Note that the polarity of particulate OM phase in *Case 3* was expected to increase, then using $K_{\mathrm{OW}}$ to calculate the distribution of polyols between organic and aqueous phases might lead to underestimated $K^{\mathrm{m}}_{\mathrm{p,OM}}$

and overestimated $K^{m}_{H,e}$. For comparison purposes, the Henry's law coefficient in pure water at 25 $^{o}$C ($K^{*}_{H,w}$) was estimated using EPI and SPARC (Hilal et al., 2008; http://archemcalc.com/sparc-web/calc), respectively (Table S4), and was adjusted for each sampling interval due to the changes in ambient temperature using van 't Hoff equation (Text S4).

***Uncertainty estimation.*** To obtain the uncertainty associated with the calculation of *F*% and partitioning coefficients ($K^{m}_{p,OM}$ and $K^{m}_{H,e}$), measurement uncertainties of polyol tracers in filter and PUF samples were estimated from their recoveries and breakthrough for gaseous sampling. The root sum of squares (RSS) method was applied to propagate uncertainties of gas and particle-phase concentrations for *F*%, $K^{m}_{p,OM}$, and $K^{m}_{H,e}$ calculations. Details of the uncertainty estimation and propagation methods were provided in Text S5, and the average relative uncertainties were summarized in Table S5.

## 3 Results and discussion

### *3.1 Method evaluation*

In our previous study, PUF/XAD-4 resin/PUF and PUF/XAD-7 resin/PUF adsorbent sandwiches were tested for sampling gaseous 2-methyltetrols and levoglucosan (Xie et al., 2014b). The results of breakthrough experiments suggested that both the two sandwiched composites had high sampling efficiency (close to 100%). Moreover, individual parts of the two types of composites (top PUF, middle XAD-4/XAD-7 resin, and backup PUF) were analyzed for 7 samples, and target compounds were only detected in top PUF. It is therefore suitable to collect gaseous 2-methylterols and levoglucosan using PUF materials only.

Although PUF materials were pre-cleaned prior to sampling, a few short-chain

315 polyurethanes or impurities could be dissolved during Soxhlet extraction of target
316 compounds using the mixture of methanol and methylene chloride. These substances
317 precipitated when sample extracts were concentrated (Figure S1a, b), and re-dissolved
318 in BSTFA:TMCS/pyridine and hexane after the derivatization step (Figure S1c, d). In
319 Xie et al. (2014b), an aliquot of 2 μL of the sample extract as shown in Figure S1d
320 was injected for GC-MS analysis. Since the dissolved PUF materials did not vaporize
321 at ~300 $^{o}$C, the GC inlet liner had to be changed for cleaning every few samples. In
322 this work, 50 μL of pure water was added to separate PUF materials from polyol
323 derivatives in hexane solution. As shown in Figure S1e, all PUF residues were
324 retained in the aqueous solution after phase separation. This pretreatment step was
325 added for the analysis of gaseous samples to save time for changing and cleaning GC
326 inlet liners. However, the revised method did not improve the recoveries of meso-
327 erythritol and levoglucosan in PUF samples (Table S2) compared to those in Xie et al.
328 (2014b). This is because the dissolved PUF materials should have an impact on the
329 derivatization efficiency of polyol species, and future work is warranted to remove
330 dissolved PUF materials in sample extracts before the derivatization step.
331 Measurement results of breakthrough samples and the resulting *B* values were
332 shown in Figure S2. C5-alkene triols and 2-methyltetrols were mainly observed in
333 summertime, and levoglucosan was only detected in three pairs of breakthrough
334 samples. Their average *B* values (< 33%) indicated no excessive breakthrough (Figure
335 S2a-c), but were higher than those reported by Xie et al. (2014b). This might be
336 ascribed to the greater face velocity (1.5 cm $s^{-1}$) for sampling gaseous polyols than
337 that (0.61 cm $s^{-1}$) in our previous study. Due to the limit in sample number for
338 breakthrough tests and low detection rates, the dependence of breakthrough on

ambient temperature or OM loadings cannot be evaluated. The breakthrough of an ideal sampling method is expected to be extremely low (e.g., <10%) and have no dependence on ambient temperature, OM loadings, etc. Unlike fructose which had low breakthrough (Figure S2d), glucose and mannitol had comparable concentrations between front and backup PUF samples for several breakthrough experiments (Figure S2e, f), indicating that PUF materials are not suitable for sampling gaseous glucose and mannitol. Mannose and arabitol were not detected or had BDL values for breakthrough samples, and their breakthrough was not provided. In the current work, concentrations of polyol tracers in filter and PUF samples were all reported, but the data of mannose, glucose, arabitol, and mannitol in PUF samples should be treated with caution due to high breakthrough or the lack of valid breakthrough results.

### *3.2 General description of measurement results*

Total ambient concentrations ($Q_f$ + $Q_b$ + PUF) of individual polyols are depicted using boxplots in Figure 2. Figure S3 presents temporal variations of total and $Q_f$ concentrations of individual polyols with daytime and night-time measurements distinguished. In general, polyol tracers were predominantly observed on $Q_f$ with averages 1-3 orders of magnitude higher than those on $Q_b$ and PUF (Table S3). Levoglucosan had the highest average total concentration (66.1 ± 71.1 ng $m^{-3}$), followed by fructose (15.0 ± 62.9 ng $m^{-3}$) and mannose (14.3 ± 31.3 ng $m^{-3}$). C5-alkene triols and 2-methyltetrols are formed from isoprene epoxydiols (IEPOX) under low $NO_X$ conditions (Surratt et al., 2010). All the five species on $Q_b$ were more frequently detected and had average concentrations 2-20 times higher than those in PUF samples. While in Xie et al. (2014b), the sum of 2-methyltetrols in $Q_b$ and adsorbent samples were up to 2.7 times higher than those on $Q_f$ in summer Denver, so

isoprene products are not similarly distributed between gas and aerosol phases across different regions. Moreover, isoprene-derived polyols exhibited prominent elevations in summer (Figure S3a-e), and their daytime concentrations (2.02 ± 3.73 – 10.5 ± 29.3 ng $m^{-3}$) were only slightly higher than those during night-time (1.63 ± 4.40 – 9.65 ± 32.7 ng $m^{-3}$). Previous field studies observed strong diurnal variations of isoprene SOA tracers with peak concentrations from afternoon till midnight (Fu and Kawamura, 2011; Isaacman-VanWertz et al., 2016). Although no IEPOX will be generated from the oxidation of isoprene by •OH and $HO_2$• after sunset, the formations of C5-alkene triols and 2-methyltetrols might continue until pre-existing IEPOX is exhausted. In this work, neither the daytime (8:00 AM–7:00 PM) or night-time (7:00 AM–7:00 AM next day) sample covered the whole period when isoprene SOA tracers had peak concentrations, and the strong diurnal variations of C5-alkene triols and 2-methyltetrols were not captured.

Levoglucosan was more frequently detected but far less concentrated in PUF than in $Q_b$ samples. Its total concentrations were comparable to those in urban Denver (average 65.3 ± 96.8 ng $m^{-3}$, range 2.48 – 478 ng $m^{-3}$), where an average of ~20% partitioned into the gas phase (Xie et al., 2014b). Due to the enhanced biomass burning activities in cold periods for domestic heating at night, levoglucosan showed a clear seasonal pattern (winter maxima and summer minima) and significant ($p$ = 0.03) higher concentrations during night-time (Figure S3f). Sugars and sugar alcohols are commonly linked with soil/dust resuspension and associated microbial activities (Simoneit et al., 2004). They were frequently detected in $Q_b$ samples with comparable averages and ranges as those in PUF samples (Table S3). Total concentrations of fructose and glucose were strongly ($r$ = 0.98) correlated peaking in middle spring

(April 2019, Figure S3h, j), when $Ca^{2+}$ on $Q_f$ also reached its maxima of the year (Yang et al., 2021), indicating an influence from soil/dust resuspension. Arabitol and mannitol had identical seasonal pattern ($r$ = 0.89) with elevated total concentrations from May to October (Figure S3i, m), which might be attributed to high levels of vegetation during growing seasons and autumn decomposition (Burshtein et al., 2011). Multiple peaks of mannose concentrations were observed from spring to autumn, suggesting a variety of contributing sources (e.g., microbial activity, vegetation). Xylitol is likely derived from biomass burning in northern Nanjing due to its strong correlation ($r$ = 0.89) with levoglucosan.

### *3.3 Gas- and particle-phase distributions*

As mentioned in sections 2.3, concentrations of particulate polyols were obtained directly from $Q_f$ measurements, and the gas phase was calculated as the sum of $Q_b$ and PUF values. Figure S4 shows the time series of gas-phase concentrations and particle-phase fractions ($F$%) of individual polyol tracers. The average $F$% values of measured species are plotted against the logarithms of their liquid-state vapor pressures at 25 °C ($p^{o,*}_L$) in Figure 3. Gas-phase C5-alkene triols and 2-methyltetrols had maximum concentrations in summer and significant ($p < 0.05$) day-night variations (Figure S4), while other polyols had extremely low concentrations in the gas phase with $F$% (average ± standard deviation) ranging from 94.2 ± 8.02 – 99.8 ± 1.21%. The average $F$% values of 2-methyltetrols (87.5 ± 10.6%) and levoglucosan (99.8 ± 1.21%) were greater than those in urban Denver (50–80%; Xie et al., 2014b), where the average sampling temperature (12.5 ± 10.1 °C) was much lower. Thus, the changes in vapor pressures with the ambient temperature and/or particulate OM loadings might not be the main factors driving gas-particle partitioning of polyol tracers in Nanjing. In

Figure 3, the average $F$% uncertainties (6.16–31.2%) of monosaccharides (e.g., fructose) and sugar alcohols (e.g., mannitol) were larger than those of isoprene SOA tracers and levoglucosan (3.33–7.24%) due to their low and variable recoveries (Table S2) and excessive breakthrough (Figure S2). However, the estimated uncertainties of $F$% for less volatile polyols ($p^{o,*}_L$ < ~$10^{-10}$ atm) were not physically meaningful, as more than 95% of these compounds existed in the particle phase. Considering the uncertainties in $F$% and log $p^{o,*}_L$ and high average $F$% (> 85%) of target polyol tracers, a dependence of $F$% on the vapor pressure could not be determined, and the seasonality and day-night difference ($p$ > 0.05) of $F$% were obscured.

### *3.4 Partitioning coefficients of gas versus organic phases*

To understand if particulate OM is the only absorbing phase in aerosols for polyol tracers in Nanjing, the absorptive partitioning coefficients of gas vs. organic phases were calculated based on measurement results ($K^m_{p,OM}$) for predefined *Cases 1-3* and predicted theoretically ($K^t_{p,OM}$) using eq. 3 and vapor pressures listed in Table S4. In Table 1, $K^t_{p,OM}$ ranges of isoprene SOA tracers, levoglucosan, and meso-erythritol are within two orders of magnitude, while those of monosaccharides and mannitol are larger (> $10^3$).When particulate OM was assumed as the only absorbing phase (*Case 1*), the average $K^m_{p,OM}$ of isoprene SOA tracers, levolgucosan, and meso-erythritol were more than 10 times greater than most of their $K^t_{p,OM}$ (Table 1), and this difference was not likely susceptible to measurement uncertainties. As shown in Table S5, the average relative uncertainties of measurement-based partitioning coefficients are all <50%, leading to an uncertainty of log $K^m_{p,OM}$ less than ± 0.30. Comparable or even greater (up to $10^5$) gap between $K^m_{p,OM}$ and $K^t_{p,OM}$ has been observed for carbonyls in a number of laboratory and field studies (Healy et al., 2008; Zhao et al.,

2013; Shen et al., 2018), which could be ascribed to reactive uptake (e.g., hydration, oligomerization, and esterification) of organic gases onto condensed phase (Galloway et al., 2009). Oligomers, sulfate and nitrate esters of 2-methyltetrols can be formed in the aerosol phase (Surratt et al., 2010; Lin et al., 2014), and their decomposition and hydrolysis during filter analysis will lead to an overestimation of particle-phase concentrations (Lin et al., 2013; Cui et al., 2018). However, the occurrence of oligomers, sulfate or nitrate esters of levoglucosan was not ever reported in ambient aerosols, although it can be readily oxidized by •OH in the aqueous phase of atmospheric particles (Hennigan et al., 2010; Hoffmann et al., 2010).

When solubility in aerosol liquid water was considered by assuming a LLPS in ambient aerosols, and whenever WSOM and WIOM partitioned into separate (*Case 2*) or single (*Case 3*) liquid phases, the average log $K^{m}_{p,OM}$ of the above mentioned compounds became much closer to or even lay within the range (e.g., levoglucosan) of log $K^{t}_{p,OM}$ (Table 1). These results indicated that the aerosol liquid water (21.3 ± 24.2 μg $m^{-3}$; Table S1) is also an important absorbing phase of ambient polyol tracers in Nanjing. Similarly, the measured average *F*% of isoprene SOA tracers in southeastern US and central Amazonia were higher than predictions by assuming instantaneous equilibrium between the gas phase and particulate OM only, and the agreement was improved when parameterization of solubility was included for predictions (Isaacman-VanWertz et al., 2016). But none of these two studies could reasonably predict the temporal variability of *F*% or log $K^{m}_{p,OM}$. One possible explanation is that the activity coefficients of isoprene SOA tracers and levoglucosan deviate from unity (0.42–2.04; Pye et al., 2018) and vary with PM composition. Pye et al. (2018) re-analyzed the measurement data from Isaacman-VanWertz et al. (2016)

using a thermodynamic equilibrium gas-particle partitioning model in two LLPS modes, which involved organic-inorganic interactions and estimations of activity coefficients as a function of liquid PM mixture composition. The resulting predictions captured both the average and diurnal variations of measured *F*% for polyol tracers, suggesting a necessity in obtaining time-resolved activity coefficients for the implementation of absorptive equilibrium partitioning model.

Unlike isoprene SOA tracers and levoglucosan, the average $K^{t}_{p,OM}$ values of monosaccharides (fructose, mannose, and glucose) and sugar alcohols (xylitol, arabitol, and mannitol) were orders of magnitude larger than their $K^{m}_{p,OM}$ for *Cases 2 and 3* (Table 1). This is probably caused by the overestimation of gas-phase concentrations of sugar polyols. The organic matter on $Q_b$ is mainly composed of volatile and semi-volatile organic compounds. If the concentrations of organic compounds on $Q_b$ were comparable or higher than those on $Q_f$, their $Q_f$ values should be dominated by positive artifact. As the vapor pressure decreases, the evaporation loss from $Q_f$ samples becomes non-negligible. Note that the magnitude of negative artifacts is unknown and very difficult to assess, and the vapor pressures of monosaccharides and sugar alcohols are far below $10^{-10}$ atm (Table S4), their concentrations in $Q_b$ and even PUF samples might contain more contributions from negative artifacts than isoprene SOA tracers and levoglucosan. As low-volatile sugar polyols had lower and less stable recoveries (Table S2) and greater breakthrough (Figure S2e, f), caution is warranted in analyzing their $K^{m}_{p,OM}$ values obtained in this study.

### *3.5 Partitioning coefficients of gas versus aqueous phases*

The predicted Henery's law coefficients in pure water ($K^{t}_{H,w}$, mol $m^{-3}$ $atm^{-1}$)

from EPI and SPARC estimates differed by several orders of magnitude, but literature values of isoprene SOA and levoglucosan were closer to EPI estimates (Table S4). If SPARC $K^{*}_{H,w}$ values were used, the average log $K^{m}_{H,e}$ of most polyol tracers would be lower than their average log $K^{t}_{H,w}$ (Table 2), indicating that the aqueous phase of ambient aerosol is less hospital to polyol tracers than pure water. This is in conflict with the fact that the interactions of organic compounds, water, and inorganic ions in aerosols will increase the partitioning of highly oxygenated compounds (O:C$\geqslant$0.6; e.g., isoprene SOA tracers and levoglucosan) into the particle phase (Pye et al., 2018). Several studies identified a close relationship between salt concentrations of aerosol water and enhanced uptake of very polar compounds (Almeida et al., 1983; Kroll et al., 2005; Ip et al., 2009; Kampf et al., 2013; Shen et al., 2018). Thus, log $K^{t}_{H,w}$ values of EPI estimates were used for further data analysis.

In Table 2, the $K^{t}_{H,w}$ values of isoprene SOA tracers, levoglucosan, and meso-erythritols based on EPI estimations were $10^{2}$ to $10^{6}$ lower than their corresponding $K^{m}_{H,e}$. Log $K^{m}_{H,e}$ values of *Cases 2* and *3* had ignorable difference and were not presented separately. Other polyol compounds exhibited less difference between log $K^{m}_{H,e}$ and log $K^{t}_{H,w}$, which was very likely caused by the overestimation of their gas-phase concentrations. The average $K^{m}_{H,e}$ values of polyol tracers ($10^{13}$–$10^{15}$ mol m$^{-3}$ atm$^{-1}$) in this study were several orders of magnitude larger than those of carbonyls derived from ambient measurements ($10^{10}$–$10^{12}$ mol m$^{-3}$ atm$^{-1}$; Shen et al., 2018) and chamber simulations (~$10^{11}$ mol m$^{-3}$ atm$^{-1}$; Kroll et al., 2005; Volkamer et al., 2006; Galloway et al., 2009). This is because low molecular weight carbonyls (e.g., glyoxal) are much more volatile ($p^{o,*}_{L}$ > $10^{-2}$ atm) than our target polyols (Table S4). According to existing studies, the minimum concentrations of gas-phase glyoxal and

methylglyoxal in Chinese cities (~0.1 μg $m^{-3}$) are magnitudes higher than the averages of polyol tracers in this work, while their particle-phase concentrations are of the same magnitude (Shen et al., 2018; Liu et al., 2020).

A number of previous studies observed enhanced $K_{H,e}$ of carbonyls with salt concentrations in aqueous solution (Ip et al., 2009; Kampf et al., 2013; Waxman et al., 2015; Shen et al., 2018), and described this "salting-in" effect using

$$\mathrm{Log}\left(\frac{K_{H,w}}{K_{H,e}}\right) = K_s c_{salt} \quad (7)$$

where $K_s$ (kg $mol^{-1}$) is the salting constant, and $c_{salt}$ is the aqueous-phase concentration of salt in mol $kg^{-1}$ ALWC. This equation is originally defined in Setschenow (1889) by plotting log ($K_{H,w}/K_{H,e}$) versus the total salt concentration (mol $L^{-1}$).

As sulfate has been identified as the major factor influencing the salting effect of carbonyl species (Kroll et al., 2005; Ip et al., 2009), Figure 4 shows modified Setschenow plots for C5-alkene triols, 2-methyltetrols, and levoglucosan, where log ($K^t_{H,w}/K^m_{H,e}$) values were regressed to the molality of sulfate ion in aerosol liquid water ($c_{sulfate}$, mol $kg^{-1}$ ALWC). The log ($K^t_{H,w}/K^m_{H,e}$) data increased faster when $c_{sulfate}$ approached 0, and deviated from their expected behavior with increased $c_{sulfate}$. Kampf et al. (2013) selected a threshold $c_{sulfate}$ of 12 mol $kg^{-1}$ ALWC to illustrate the deviation for chamber experiments, and attributed it to elevated viscosity and slow particle-phase reactions at high $c_{sulfate}$. In Figure 4, negative correlations ($p < 0.01$) are observed at $c_{sulfate}$ < 12 mol $kg^{-1}$ ALWC, and Figure S5 exhibits significant negative correlations ($p < 0.01$) between log ($K^t_{H,w}/K^m_{H,e}$) and $c_{sulfate}$ for individual polyols even without excluding the deviations at high $c_{sulfate}$. The $K_s$ values of polyol tracers from Figures 4 and S5 (-0.17 – -0.037 kg $mol^{-1}$) are in a similar range as that of glyoxal (-0.24 – -0.04 kg $mol^{-1}$; Kampf et al., 2013; Shen et al., 2018; Waxman et al., 2015).

These results indicated that the shifting of gas-particle equilibrium toward the condensed phase might be partly parameterized by the equation defining "salting-in" effects.

However, the "salting-in" effect is a known phenomenon that is not likely linked with a specific physical or chemical mechanism. Quantum chemical calculation results indicated negative Gibbs free energy of water displacement for interactions between $SO_4^{2-}$ and glyoxal monohydrate (Waxman et al., 2015). The net "salting-in" effect of 1-nitro-2-naphthol in NaF solution was interpreted by postulating hydrogen bonding (Almeida et al., 1983). A direct binding of cations to ether oxygens was proposed to be responsible for the increased solubility of water-soluble polymers (Sadeghi and Jahani, 2012). Due to the moderate correlations and negative intercepts in Figures 4 and S5, the gap between $K^{t}_{H,e}$ and $K^{m}_{H,w}$ cannot be closed by the "salting-in" effect alone. Shen et al. (2018) also obtained negative intercepts when plotting log ($K^{t}_{H,w}/K^{m}_{H,e}$) over $c_{sulfate}$ for glyoxal and methylglyoxal in ambient atmosphere, and attributed this to unknown gas-particle partitioning mechanisms. Evidences showing that the thermal degradation of less volatile oligomers and organosulfates can lead to an overestimation of 2-methyltetrols by 60–188% when using a conventional GC/EI-MS method (Cui et al., 2018). To fit the gas-particle distribution of 2-methyltetrols in southeastern US, 50% of particulate 2-methyltetrols was presumed to exist in chemical forms with much lower vapor pressures by Pye et al. (2018). So, the reactive uptake and aqueous phase chemistry could be explanations for the enhanced uptake of isoprene SOA tracers. Moreover, log ($K^{t}_{H,w}/K^{m}_{H,e}$) values of polyol tracers also negatively correlated with the aqueous-phase concentrations of WSOC ($c_{WSOC}$, Figure S6), but not $NH_4^+$ or $NO_3^-$. This dependence might be associated with the "like-

555 dissolves-like" rule, or indicate the importance of aqueous-phase heterogeneous
556 reactions (Hennigan et al., 2009; Volkamer et al., 2009). Although several studies
557 have estimated Henry's law constants for a variety of polar organic compounds in
558 pure water (e.g., polyols and polyacids; Compernolle and Müller, 2014a, b), more
559 work is warranted to decrease the estimation uncertainty and explain their increased
560 partitioning toward aerosol liquid water explicitly.

561 **4 Implications and conclusions**

562 In this work, concentrations of gas- and particle-phase polyol tracers were
563 measured simultaneously in northern Nanjing. The temporal variations of individual
564 compounds were dominated by their particle-phase concentrations. Then gas-particle
565 partitioning of polyol tracers should have little influence on source apportionment
566 based on particle-phase data in Nanjing. An improved agreement between
567 measurement-based and predicted $K_{p,OM}$ of polyol tracers was observed when the
568 solubility in aerosol liquid water was considered, indicating that the aqueous solution
569 in aerosols is also an important absorbing phase. The large gaps of $K^{m}_{H,e}$ versus $K^{t}_{H,w}$
570 could be partly parameterized using the equation defining "salting-in" effects.
571 According to existing studies, reactive uptake, aqueous phase reactions, and chemical
572 similarity between partitioning species and the absorbing phase might be responsible
573 for increasing the partitioning of polyol tracers into the condensed phase. So, the
574 results of this study have important implications on the prediction of gas-particle
575 partitioning of water-soluble organics, and further studies are required to explain their
576 enhanced aqueous-phase uptake mechanistically. Due to the hygroscopic properties of
577 highly oxidized organic aerosols, this study also partly reveals the discrepancy
578 between modeled and observed SOA in previous studies. However, several

assumptions (e.g., LLPS) were made for proposed gas-particle partitioning schemes in this work, more laboratory research is needed to understand the mixing state of inorganic salts, organic components, and aerosol liquid water in atmospheric particles.

***Data availability***

Data used in the writing of this paper is available at the Harvard Dataverse (https://doi.org/10.7910/DVN/U3IGQR, Qin et al., 2021)

***Author contributions***

MX designed the research. CQ and YG performed the sampling and chemical analysis. CQ, YM, and MX analyzed the data. CQ and MX wrote the paper with significant contributions from YW, HL, and QW.

***Competing interests***

The authors declare that they have no conflict of interest.

***Acknowledgements***

This research was supported by the National Natural Science Foundation of China (NSFC, 41701551). Y. W. was supported by the National Science Foundation Atmospheric Chemistry Program.

## References


Ahrens, L., Shoeib, M., Harner, T., Lane, D. A., Guo, R., and Reiner, E. J.: Comparison of annular diffusion denuder and high volume air samplers for measuring per- and polyfluoroalkyl substances in the atmosphere, Anal. Chem., 83, 9622-9628, 10.1021/ac202414w, 2011.

Almeida, M. B., Alvarez, A. M., Miguel, E. M. D., and Hoyo, E. S. D.: Setchenow coefficients for naphthols by distribution method, Can. J. Chem., 61, 244-248, 10.1139/v83-043, 1983.

Barsanti, K. C., and Pankow, J. F.: Thermodynamics of the formation of atmospheric organic particulate matter by accretion reactions—Part 1: aldehydes and ketones, Atmos. Environ., 38, 4371-4382, 10.1016/j.atmosenv.2004.03.035, 2004.

Bauer, H., Claeys, M., Vermeylen, R., Schueller, E., Weinke, G., Berger, A., and Puxbaum, H.: Arabitol and mannitol as tracers for the quantification of airborne fungal spores, Atmos. Environ., 42, 588-593, https://doi.org/10.1016/j.atmosenv.2007.10.013, 2008.

Burshtein, N., Lang-Yona, N., and Rudich, Y.: Ergosterol, arabitol and mannitol as tracers for biogenic aerosols in the eastern Mediterranean, Atmos. Chem. Phys., 11, 829-839, 10.5194/acp-11-829-2011, 2011.

Claeys, M., Graham, B., Vas, G., Wang, W., Vermeylen, R., Pashynska, V., Cafmeyer, J., Guyon, P., Andreae, M. O., Artaxo, P., and Maenhaut, W.: Formation of secondary organic aerosols through photooxidation of isoprene, Science, 303, 1173-1176, 10.1126/science.1092805, 2004.

Compernolle, S., and Müller, J. F.: Henry's law constants of polyols, Atmos. Chem. Phys., 14, 12815-12837, 10.5194/acp-14-12815-2014, 2014a.

Compernolle, S., and Müller, J. F.: Henry's law constants of diacids and hydroxy polyacids: recommended values, Atmos. Chem. Phys., 14, 2699-2712, 10.5194/acp-14-2699-2014, 2014b.

Cui, T., Zeng, Z., dos Santos, E. O., Zhang, Z., Chen, Y., Zhang, Y., Rose, C. A., Budisulistiorini, S. H., Collins, L. B., Bodnar, W. M., de Souza, R. A. F., Martin, S. T., Machado, C. M. D., Turpin, B. J., Gold, A., Ault, A. P., and Surratt, J. D.: Development of a hydrophilic interaction liquid chromatography (HILIC) method for the chemical characterization of water-soluble isoprene epoxydiol (IEPOX)-derived secondary organic aerosol, Environmental Science: Environ. Sci.: Process. Impacts, 20, 1524-1536, 10.1039/C8EM00308D, 2018.

Fu, P., and Kawamura, K.: Diurnal variations of polar organic tracers in summer forest aerosols: A case study of a Quercus and Picea mixed forest in Hokkaido, Japan, Geochem. J., 45, 297-308, 10.2343/geochemj.1.0123, 2011.

Galloway, M. M., Chhabra, P. S., Chan, A. W. H., Surratt, J. D., Flagan, R. C., Seinfeld, J. H., and Keutsch, F. N.: Glyoxal uptake on ammonium sulphate seed aerosol: reaction products and reversibility of uptake under dark and irradiated conditions, Atmos. Chem. Phys., 9, 3331-3345, 10.5194/acp-9-3331-2009, 2009.

Hallar, A. G., Lowenthal, D. H., Clegg, S. L., Samburova, V., Taylor, N., Mazzoleni, L. R., Zielinska, B. K., Kristensen, T. B., Chirokova, G., McCubbin, I. B., Dodson, C., and Collins, D.: Chemical and hygroscopic properties of aerosol organics at Storm Peak Laboratory, J. Geophys. Res. Atmos., 118, 4767-4779, https://doi.org/10.1002/jgrd.50373, 2013.

Heald, C. L., Jacob, D. J., Park, R. J., Russell, L. M., Huebert, B. J., Seinfeld, J. H., Liao, H., and Weber, R. J.: A large organic aerosol source in the free troposphere missing from current models, Geophys. Res. Lett., 32, L18809, https://doi.org/10.1029/2005GL023831, 2005.

Healy, R. M., Wenger, J. C., Metzger, A., Duplissy, J., Kalberer, M., and Dommen, J.: Gas/particle partitioning of carbonyls in the photooxidation of isoprene and 1,3,5-trimethylbenzene, Atmos. Chem. Phys., 8, 3215-3230, 10.5194/acp-8-3215-2008, 2008.

Hennigan, C. J., Bergin, M. H., Russell, A. G., Nenes, A., and Weber, R. J.: Gas/particle partitioning of water-soluble organic aerosol in Atlanta, Atmos. Chem. Phys., 9, 3613-3628, 10.5194/acp-9-3613-2009, 2009.

Hennigan, C. J., Sullivan, A. P., Collett Jr, J. L., and Robinson, A. L.: Levoglucosan stability in biomass burning particles exposed to hydroxyl radicals, Geophys. Res. Lett., 37, L09806, https://doi.org/10.1029/2010GL043088, 2010.

Hilal, S. H., Ayyampalayam, S. N., and Carreira, L. A.: Air−liquid partition coefficient for a diverse set of organic compounds: Henry's Law constant in water and hexadecane, Environ. Sci. Technol., 42, 9231-9236, 10.1021/es8005783, 2008.

Hodzic, A., Jimenez, J. L., Madronich, S., Canagaratna, M. R., DeCarlo, P. F., Kleinman, L., and Fast, J.: Modeling organic aerosols in a megacity: potential contribution of semi-volatile and intermediate volatility primary organic compounds to secondary organic aerosol formation,

660 Atmos. Chem. Phys., 10, 5491-5514, 10.5194/acp-10-5491-2010, 2010.
661 Hoffmann, D., Tilgner, A., Iinuma, Y., and Herrmann, H.: Atmospheric stability of levoglucosan: A
662 detailed laboratory and modeling study, Environ. Sci. Technol., 44, 694-699, 10.1021/es902476f,
663 2010.
664 Hu, D., Bian, Q., Lau, A. K. H., and Yu, J. Z.: Source apportioning of primary and secondary organic
665 carbon in summer PM2.5 in Hong Kong using positive matrix factorization of secondary and
666 primary organic tracer data, J. Geophys. Res. Atmos., 115, D16204,
667 https://doi.org/10.1029/2009JD012498, 2010.
668 Ip, H. S. S., Huang, X. H. H., and Yu, J. Z.: Effective Henry's law constants of glyoxal, glyoxylic acid,
669 and glycolic acid, Geophys. Res. Lett., 36, L01802, https://doi.org/10.1029/2008GL036212, 2009.
670 Isaacman-VanWertz, G., Yee, L. D., Kreisberg, N. M., Wernis, R., Moss, J. A., Hering, S. V., de Sá, S.
671 S., Martin, S. T., Alexander, M. L., Palm, B. B., Hu, W., Campuzano-Jost, P., Day, D. A.,
672 Jimenez, J. L., Riva, M., Surratt, J. D., Viegas, J., Manzi, A., Edgerton, E., Baumann, K., Souza,
673 R., Artaxo, P., and Goldstein, A. H.: Ambient gas-particle partitioning of tracers for biogenic
674 oxidation, Environ. Sci. Technol., 50, 9952-9962, 10.1021/acs.est.6b01674, 2016.
675 Jang, M., Czoschke, N. M., Lee, S., and Kamens, R. M.: Heterogeneous atmospheric aerosol
676 production by acid-catalyzed particle-phase reactions, Science, 298, 814,
677 10.1126/science.1075798, 2002.
678 Kampf, C. J., Waxman, E. M., Slowik, J. G., Dommen, J., Pfaffenberger, L., Praplan, A. P., Prévôt, A.
679 S. H., Baltensperger, U., Hoffmann, T., and Volkamer, R.: Effective Henry's law partitioning and
680 the salting constant of glyoxal in aerosols containing sulfate, Environ. Sci. Technol., 47, 4236-
681 4244, 10.1021/es400083d, 2013.
682 Kondo, Y., Miyazaki, Y., Takegawa, N., Miyakawa, T., Weber, R. J., Jimenez, J. L., Zhang, Q., and
683 Worsnop, D. R.: Oxygenated and water-soluble organic aerosols in Tokyo, J. Geophys. Res.
684 Atmos., 112, D01203, 10.1029/2006jd007056, 2007.
685 Kroll, J. H., Ng, N. L., Murphy, S. M., Varutbangkul, V., Flagan, R. C., and Seinfeld, J. H.: Chamber
686 studies of secondary organic aerosol growth by reactive uptake of simple carbonyl compounds, J.
687 Geophys. Res. Atmos., 110, D23207, https://doi.org/10.1029/2005JD006004, 2005.
688 Lin, Y.-H., Budisulistiorini, S. H., Chu, K., Siejack, R. A., Zhang, H., Riva, M., Zhang, Z., Gold, A.,
689 Kautzman, K. E., and Surratt, J. D.: Light-absorbing oligomer formation in secondary organic
690 aerosol from reactive uptake of isoprene epoxydiols, Environ. Sci. Technol., 48, 12012-12021,
691 10.1021/es503142b, 2014.
692 Lin, Y. H., Knipping, E. M., Edgerton, E. S., Shaw, S. L., and Surratt, J. D.: Investigating the
693 influences of SO2 and NH3 levels on isoprene-derived secondary organic aerosol formation using
694 conditional sampling approaches, Atmos. Chem. Phys., 13, 8457-8470, 10.5194/acp-13-8457-
695 2013, 2013.
696 Liu, J., Li, X., Li, D., Xu, R., Gao, Y., Chen, S., Liu, Y., Zhao, G., Wang, H., Wang, H., Lou, S., Chen,
697 M., Hu, J., Lu, K., Wu, Z., Hu, M., Zeng, L., and Zhang, Y.: Observations of glyoxal and
698 methylglyoxal in a suburban area of the Yangtze River Delta, China, Atmos. Environ., 238,
699 117727, https://doi.org/10.1016/j.atmosenv.2020.117727, 2020.
700 Odum, J. R., Hoffmann, T., Bowman, F., Collins, D., Flagan, R. C., and Seinfeld, J. H.: Gas/particle
701 partitioning and secondary organic aerosol yields, Environ. Sci. Technol., 30, 2580-2585,
702 10.1021/es950943+, 1996.
703 Pankow, J. F.: An absorption model of the gas/aerosol partitioning involved in the formation of
704 secondary organic aerosol, Atmos. Environ., 28, 189-193, 10.1016/1352-2310(94)90094-9, 1994a.
705 Pankow, J. F.: An absorption model of gas/particle partitioning of organic compounds in the
706 atmosphere, Atmos. Environ., 28, 185-188, 10.1016/1352-2310(94)90093-0, 1994b.
707 Perraud, V., Bruns, E. A., Ezell, M. J., Johnson, S. N., Yu, Y., Alexander, M. L., Zelenyuk, A., Imre,
708 D., Chang, W. L., Dabdub, D., Pankow, J. F., and Finlayson-Pitts, B. J.: Nonequilibrium
709 atmospheric secondary organic aerosol formation and growth, Proc. Natl. Acad. Sci. U.S.A., 109,
710 2836-2841, 10.1073/pnas.1119909109, 2012.
711 Peters, A. J., Lane, D. A., Gundel, L. A., Northcott, G. L., and Jones, K. C.: A comparison of high
712 volume and diffusion denuder samplers for measuring semivolatile organic compounds in the
713 atmosphere, Environ. Sci. Technol., 34, 5001-5006, 10.1021/es000056t, 2000.
714 Pye, H. O. T., Zuend, A., Fry, J. L., Isaacman-VanWertz, G., Capps, S. L., Appel, K. W., Foroutan, H.,
715 Xu, L., Ng, N. L., and Goldstein, A. H.: Coupling of organic and inorganic aerosol systems and
716 the effect on gas–particle partitioning in the southeastern US, Atmos. Chem. Phys., 18, 357-370,
717 10.5194/acp-18-357-2018, 2018.

Qin, C., Gou, Y., Wang, Y., Mao, Y., Liao, H., Wang, Q. g., and Xie, M.: Replication Data for: Gas-particle partitioning of polyol tracers in the western Yangtze River Delta, China, in, V1 ed., Harvard Dataverse, https://doi.org/10.7910/DVN/U3IGQR, 2021.

Sadeghi, R., and Jahani, F.: Salting-in and salting-out of water-soluble polymers in aqueous salt solutions, J. Phys. Chem. B, 116, 5234-5241, 10.1021/jp300665b, 2012.

Saxena, P., and Hildemann, L.: Water-soluble organics in atmospheric particles: A critical review of the literature and application of thermodynamics to identify candidate compounds, J. Atmos. Chem., 24, 57-109, 10.1007/bf00053823, 1996.

Setschenow, J.: Über die Konstitution der Salzlösungen auf Grund ihres Verhaltens zu Kohlensäure, Z. Phys. Chem., 4U, 117-125, https://doi.org/10.1515/zpch-1889-0409, 1889.

Shen, H., Chen, Z., Li, H., Qian, X., Qin, X., and Shi, W.: Gas-particle partitioning of carbonyl compounds in the ambient atmosphere, Environ. Sci. Technol., 52, 10997-11006, 10.1021/acs.est.8b01882, 2018.

Simcik, M. F., Franz, T. P., Zhang, H., and Eisenreich, S. J.: Gas-particle partitioning of PCBs and PAHs in the Chicago urban and adjacent coastal atmosphere: States of equilibrium, Environ. Sci. Technol., 32, 251-257, 10.1021/es970557n, 1998.

Simoneit, B. R. T., Schauer, J. J., Nolte, C. G., Oros, D. R., Elias, V. O., Fraser, M. P., Rogge, W. F., and Cass, G. R.: Levoglucosan, a tracer for cellulose in biomass burning and atmospheric particles, Atmos. Environ., 33, 173-182, http://dx.doi.org/10.1016/S1352-2310(98)00145-9, 1999.

Simoneit, B. R. T., Elias, V. O., Kobayashi, M., Kawamura, K., Rushdi, A. I., Medeiros, P. M., Rogge, W. F., and Didyk, B. M.: Sugars dominant water-soluble organic compounds in soils and characterization as tracers in atmospheric particulate matter, Environ. Sci. Technol., 38, 5939-5949, 10.1021/es0403099, 2004.

Surratt, J. D., Murphy, S. M., Kroll, J. H., Ng, N. L., Hildebrandt, L., Sorooshian, A., Szmigielski, R., Vermeylen, R., Maenhaut, W., Claeys, M., Flagan, R. C., and Seinfeld, J. H.: Chemical composition of secondary organic aerosol formed from the photooxidation of isoprene, J. Phys. Chem. A, 110, 9665-9690, 10.1021/jp061734m, 2006.

Surratt, J. D., Chan, A. W. H., Eddingsaas, N. C., Chan, M., Loza, C. L., Kwan, A. J., Hersey, S. P., Flagan, R. C., Wennberg, P. O., and Seinfeld, J. H.: Reactive intermediates revealed in secondary organic aerosol formation from isoprene, Proc. Natl. Acad. Sci. U.S.A., 107, 6640-6645, 10.1073/pnas.0911114107, 2010.

Taylor, N. F., Collins, D. R., Lowenthal, D. H., McCubbin, I. B., Hallar, A. G., Samburova, V., Zielinska, B., Kumar, N., and Mazzoleni, L. R.: Hygroscopic growth of water soluble organic carbon isolated from atmospheric aerosol collected at US national parks and Storm Peak Laboratory, Atmos. Chem. Phys., 17, 2555-2571, 10.5194/acp-17-2555-2017, 2017.

Tsyro, S. G.: To what extent can aerosol water explain the discrepancy between model calculated and gravimetric PM10 and PM2.5?, Atmos. Chem. Phys., 5, 515-532, 10.5194/acp-5-515-2005, 2005.

Turpin, B. J., and Lim, H.-J.: Species contributions to PM2.5 mass concentrations: Revisiting common assumptions for estimating organic mass, Aerosol Sci. Technol., 35, 602-610, 10.1080/02786820119445, 2001.

US EPA: Estimation Program Interface (EPI) Suite. Version v4.11, 2012. United States Environmental Protection Agency, Washington, DC, USA. https://www.epa.gov/tsca-screening-tools/download-epi-suitetm-estimation-program-interface-v411

Volkamer, R., Jimenez, J. L., San Martini, F., Dzepina, K., Zhang, Q., Salcedo, D., Molina, L. T., Worsnop, D. R., and Molina, M. J.: Secondary organic aerosol formation from anthropogenic air pollution: Rapid and higher than expected, Geophys. Res. Lett., 33, L17811, https://doi.org/10.1029/2006GL026899, 2006.

Volkamer, R., Ziemann, P. J., and Molina, M. J.: Secondary Organic Aerosol Formation from Acetylene (C2H2): seed effect on SOA yields due to organic photochemistry in the aerosol aqueous phase, Atmos. Chem. Phys., 9, 1907-1928, 10.5194/acp-9-1907-2009, 2009.

Wang, W., Kourtchev, I., Graham, B., Cafmeyer, J., Maenhaut, W., and Claeys, M.: Characterization of oxygenated derivatives of isoprene related to 2-methyltetrols in Amazonian aerosols using trimethylsilylation and gas chromatography/ion trap mass spectrometry, Rapid Commun. Mass Spectrom., 19, 1343-1351, https://doi.org/10.1002/rcm.1940, 2005.

Waxman, E. M., Elm, J., Kurtén, T., Mikkelsen, K. V., Ziemann, P. J., and Volkamer, R.: Glyoxal and methylglyoxal Setschenow salting constants in sulfate, nitrate, and chloride solutions: Measurements and Gibbs energies, Environ. Sci. Technol., 49, 11500-11508, 10.1021/acs.est.5b02782, 2015.

Williams, B. J., Goldstein, A. H., Kreisberg, N. M., and Hering, S. V.: In situ measurements of gas/particle-phase transitions for atmospheric semivolatile organic compounds, Proc. Natl. Acad. Sci. U.S.A., 107, 6676-6681, 10.1073/pnas.0911858107, 2010.

Xie, M., Barsanti, K. C., Hannigan, M. P., Dutton, S. J., and Vedal, S.: Positive matrix factorization of PM2.5 - eliminating the effects of gas/particle partitioning of semivolatile organic compounds, Atmos. Chem. Phys., 13, 7381-7393, 10.5194/acp-13-7381-2013, 2013.

Xie, M., Hannigan, M. P., and Barsanti, K. C.: Gas/particle partitioning of n-alkanes, PAHs and oxygenated PAHs in urban Denver, Atmos. Environ., 95, 355-362, http://dx.doi.org/10.1016/j.atmosenv.2014.06.056, 2014a.

Xie, M., Hannigan, M. P., and Barsanti, K. C.: Gas/particle partitioning of 2-methyltetrols and levoglucosan at an urban site in Denver, Environ. Sci. Technol., 48, 2835-2842, 10.1021/es405356n, 2014b.

Xie, M., Hannigan, M. P., and Barsanti, K. C.: Impact of gas/particle partitioning of semivolatile organic compounds on source apportionment with positive matrix factorization, Environ. Sci. Technol., 48, 9053-9060, 10.1021/es5022262, 2014c.

Yang, L., Shang, Y., Hannigan, M. P., Zhu, R., Wang, Q. g., Qin, C., and Xie, M.: Collocated speciation of PM2.5 using tandem quartz filters in northern nanjing, China: Sampling artifacts and measurement uncertainty, Atmos. Environ., 246, 118066, https://doi.org/10.1016/j.atmosenv.2020.118066, 2021.

Yatavelli, R. L. N., Stark, H., Thompson, S. L., Kimmel, J. R., Cubison, M. J., Day, D. A., Campuzano-Jost, P., Palm, B. B., Hodzic, A., Thornton, J. A., Jayne, J. T., Worsnop, D. R., and Jimenez, J. L.: Semicontinuous measurements of gas–particle partitioning of organic acids in a ponderosa pine forest using a MOVI-HRToF-CIMS, Atmos. Chem. Phys., 14, 1527-1546, 10.5194/acp-14-1527-2014, 2014.

Zhang, Y., Sheesley, R. J., Schauer, J. J., Lewandowski, M., Jaoui, M., Offenberg, J. H., Kleindienst, T. E., and Edney, E. O.: Source apportionment of primary and secondary organic aerosols using positive matrix factorization (PMF) of molecular markers, Atmos. Environ., 43, 5567-5574, https://doi.org/10.1016/j.atmosenv.2009.02.047, 2009.

Zhao, Y., Kreisberg, N. M., Worton, D. R., Isaacman, G., Weber, R. J., Liu, S., Day, D. A., Russell, L. M., Markovic, M. Z., VandenBoer, T. C., Murphy, J. G., Hering, S. V., and Goldstein, A. H.: Insights into secondary organic aerosol formation mechanisms from measured gas/particle partitioning of specific organic tracer compounds, Environ. Sci. Technol., 47, 3781-3787, 10.1021/es304587x, 2013.

Zuend, A., and Seinfeld, J. H.: Modeling the gas-particle partitioning of secondary organic aerosol: the importance of liquid-liquid phase separation, Atmos. Chem. Phys., 12, 3857-3882, 10.5194/acp-12-3857-2012, 2012.

Table 1. Comparisons of measurement-based log $K_{p,OM}$ ($m^3\ \mu g^{-1}$) at three proposed cases and predicted values.

| Species | No. of obs. | Log $K^m_{p,OM}$ [a] | | | Log $K^t_{p,OM}$ [b] | | | |
|---|---|---|---|---|---|---|---|---|
| | | Case 1 | Case 2 | Case 3 | EPI | EVAPORATION | SPARC | SIMPOL |
| ***Isoprene SOA tracers*** | | | | | | | | |
| C5-alkene triol 1 | 53 | 0.33 ± 0.71 | -0.79 ± 0.86 | -0.82 ± 0.85 | -3.09 | -2.84 | -1.19 | -2.88 |
| C5-alkene triol 2 | 63 | 0.15 ± 0.55 | -1.02 ± 0.74 | -1.05 ± 0.73 | -3.62 | -3.67 | -4.14 | -2.85 |
| C5-alkene triol 3 | 83 | 0.35 ± 0.68 | -0.83 ± 0.86 | -0.86 ± 0.85 | -2.90 | -2.65 | -1.00 | -2.69 |
| 2-Methylthreitol | 101 | -0.12 ± 0.48 | -2.09 ± 0.71 | -2.09 ± 0.70 | -1.87 | -1.30 | -1.18 | -0.47 |
| 2-Methylerythritol | 95 | -0.011 ± 0.58 | -1.96 ± 0.71 | -1.96 ± 0.71 | -1.90 | -1.34 | -1.22 | -0.50 |
| ***Biomass burning tracer*** | | | | | | | | |
| Levoglucosan | 65 | 2.23 ± 0.72 | 0.63 ± 0.90 | 0.62 ± 0.90 | -0.04 | -0.81 | 1.04 | -0.76 |
| ***Sugars ang sugar alcohols*** | | | | | | | | |
| Meso-erythritol | 31 | 0.87 ± 0.53 | -1.43 ± 0.60 | -1.43 ± 0.60 | -0.65 | -1.21 | -0.45 | |
| Fructose | 85 | 0.65 ± 0.73 | -1.20 ± 0.83 | -1.20 ± 0.89 | 1.17 | 2.76 | 6.94 | |
| Mannose | 74 | 0.62 ± 0.71 | -2.12 ± 0.95 | -2.12 ± 0.95 | 1.28 | 2.13 | 4.77 | |
| Glucose | 88 | 0.42 ± 0.67 | -2.77 ± 0.93 | -2.77 ± 0.93 | 0.34 | 3.75 | 7.32 | |
| Xylitol | 22 | 0.24 ± 0.54 | -2.61 ± 0.72 | -2.61 ± 0.72 | 3.37 | 2.34 | 3.57 | |
| Arabitol | 30 | 1.46 ± 0.89 | -1.35 ± 1.24 | -1.35 ± 1.24 | 3.25 | 1.67 | 2.90 | |
| Manitol | 65 | 1.08 ± 0.63 | -2.24 ± 0.95 | -2.24 ± 0.95 | 2.33 | 4.16 | 6.68 | |

[a] Average ± standard deviation; [b] temperature range: -4~36 °C.

Table 2. Comparisons of measurement-based log $K_{H,e}$ (mol $m^{-3}$ $atm^{-1}$) and predicted log $K_{H,w}$ of individual polyol tracers.

| Species | No. of obs. | Log $K^{m}_{H,e}$ (Cases 2)[a] | | | Log $K^{t}_{H,w}$[b] | |
|---|---|---|---|---|---|---|
| | | Median | Average | Range | EPI | SPARC |
| ***Isoprene SOA tracers*** | | | | | | |
| C5-alkene triol 1 | 53 | 14.0 | 13.9 ± 0.86 | 11.5 – 16.4 | 7.22 | 11.7 |
| C5-alkene triol 2 | 63 | 13.7 | 13.6 ± 0.73 | 11.2 – 16.1 | 7.34 | 7.66 |
| C5-alkene triol 3 | 83 | 13.9 | 13.8 ± 0.85 | 10.6 – 16.1 | 7.43 | 11.9 |
| 2-Methylthreitol | 101 | 13.4 | 13.3 ± 0.70 | 10.9 – 14.8 | 10.0 | 14.1 |
| 2-Methylerythritol | 95 | 13.5 | 13.5 ± 0.71 | 11.6 – 15.6 | 9.95 | 14.1 |
| ***Biomass burning tracer*** | | | | | | |
| Levoglucosan | 65 | 15.7 | 15.7 ± 0.90 | 13.2 – 17.3 | 13.4 | 16.1 |
| ***Sugars ang sugar alcohols*** | | | | | | |
| Meso-erythritol | 31 | 14.5 | 14.4 ± 0.60 | 12.8 – 15.6 | 9.65 | 13.8 |
| Fructose | 85 | 14.2 | 14.1 ± 0.89 | 11.9 – 16.5 | 14.7 | 19.9 |
| Mannose | 74 | 14.0 | 14.1 ± 0.94 | 12.1 – 16.8 | 10.9 | 18.8 |
| Glucose | 88 | 13.9 | 13.9 ± 0.93 | 11.3 – 16.3 | 14.7 | 20.9 |
| Xylitol | 22 | 13.8 | 13.7 ± 0.72 | 12.6 – 15.0 | 12.1 | 18.1 |
| Arabitol | 30 | 15.1 | 15.0 ± 1.23 | 13.0 – 18.2 | 11.3 | 17.4 |
| Mannitol | 65 | 14.6 | 14.5 ± 0.94 | 12.1 – 16.4 | 12.9 | 20.8 |

[a] Log $K^{m}_{H,e}$ values of *Case 3* had ignorable difference, and were not exhibited separately; [b] temperature range: -4~36 $^{o}$C.

Figure 1

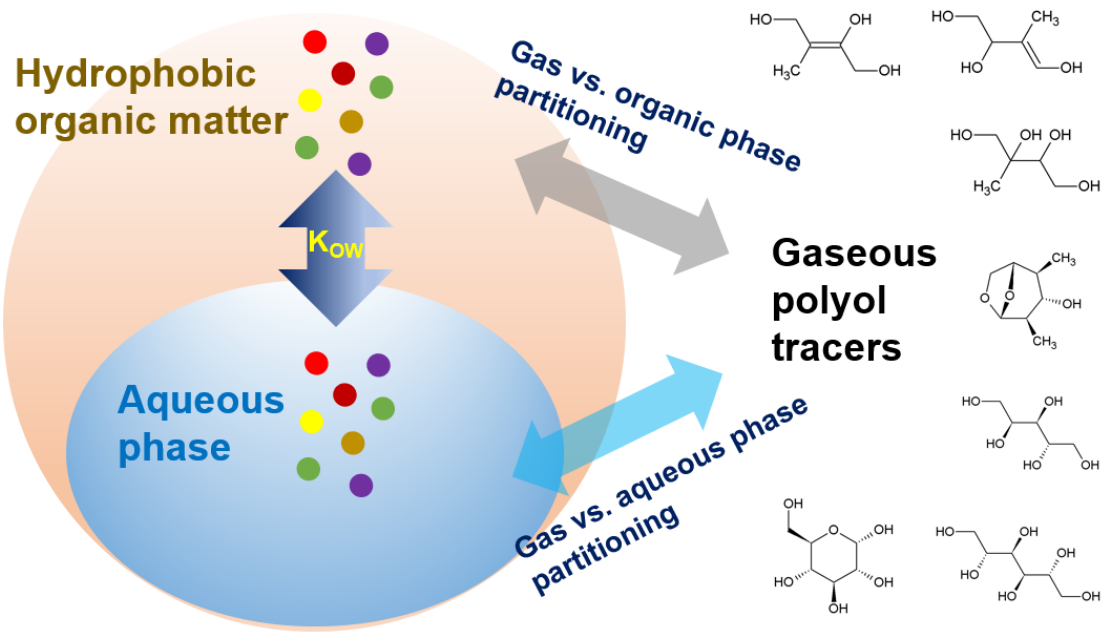


Figure 1. Proposed scheme for gas-particle partitioning of polyol tracers.

# Figure 2

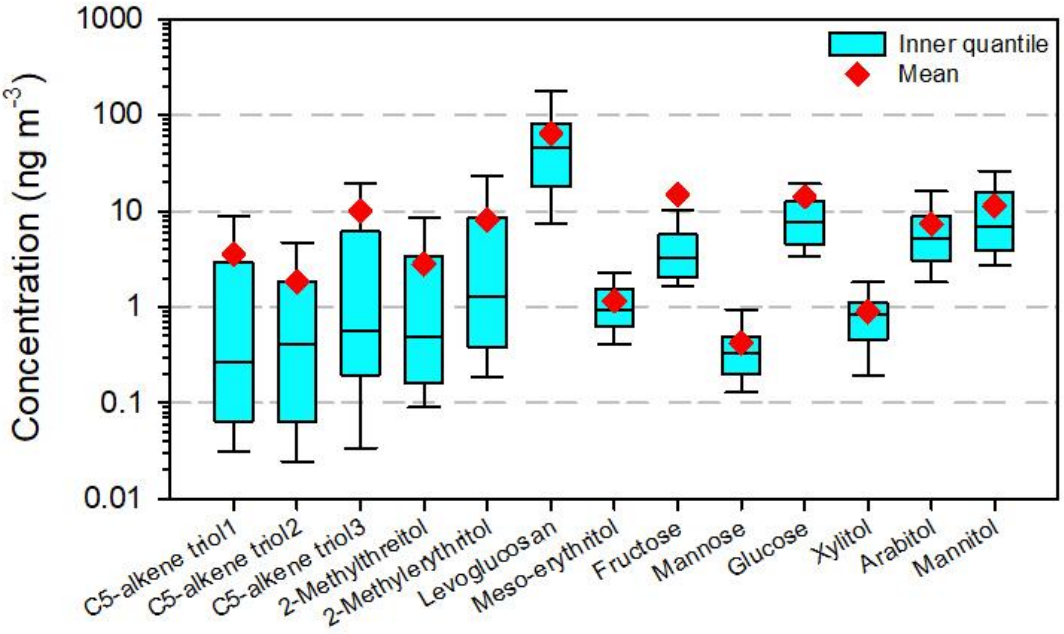


Figure 2. Total concentrations of individual polyols ($Q_f$ + $Q_b$ + PUF) in the ambient atmosphere of northern Nanjing. The boxes depict the median (dark line), inner quantile range (box), 10$^{th}$ and 90$^{th}$ percentiles (whiskers), and the mean (red diamond).

# Figure 3

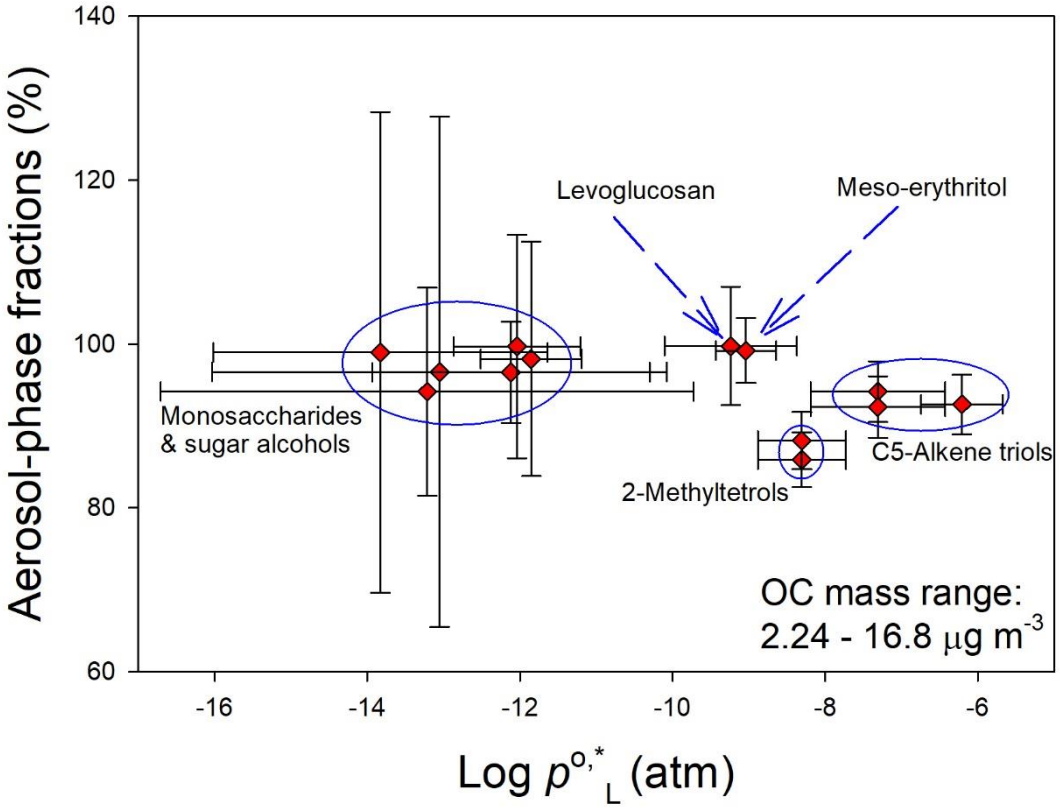


Figure 3. Average particle-phase fractions and log $p^{o,*}_L$ of individual polyol tracers. Whiskers represent uncertainties of *F*% and one standard deviation of log $p^{o,*}_L$ derived from different estimation tools.

# Figure 4

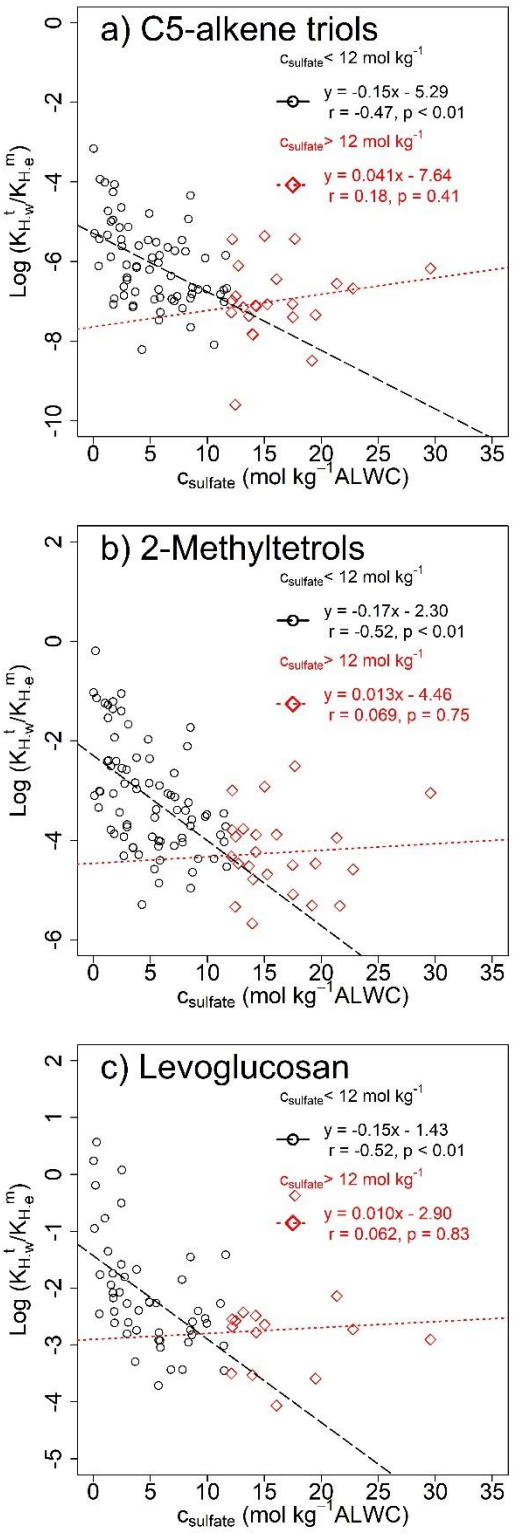


Figure 4. Modified Setschenow plots of log ($K^t_{H,w}/K^m_{H,e}$) versus $c_{sulfate}$ for (a) C5-alkene triols, (b) 2-methyltetrols, and (c) levoglucosan.